Published in final edited form as:

Nat Phys. 2023 December ; 19(12): 1927–1935.

Scaling behaviour and control of nuclear wrinkling

Jonathan A. Jackson[1,2,*], **Nicolas Romeo**[3,4,*], **Alexander Mietke**[3,5], **Keaton J. Burns**[3], **Jan F. Totz**[3], **Adam C. Martin**[1], **Jörn Dunkel**[3,†], **Jasmin Imran Alsous**[6,‡]

[1]Department of Biology, Massachusetts Institute of Technology

[2]Graduate Program in Biophysics, Harvard University

[3]Department of Mathematics, Massachusetts Institute of Technology

[4]Department of Physics, Massachusetts Institute of Technology

[5]School of Mathematics, University of Bristol

[6]Center for Computational Biology, Flatiron Institute, Simons Foundation

Abstract

The cell nucleus is enveloped by a complex membrane, whose wrinkling has been implicated in disease and cellular aging. The biophysical dynamics and spectral evolution of nuclear wrinkling during multicellular development remain poorly understood due to a lack of direct quantitative measurements. Here, we characterize the onset and dynamics of nuclear wrinkling during egg development in the fruit fly when nurse cell nuclei increase in size and display stereotypical wrinkling behavior. A spectral analysis of three-dimensional high-resolution live imaging data from several hundred nuclei reveals a robust asymptotic power-law scaling of angular fluctuations consistent with renormalization and scaling predictions from a nonlinear elastic shell model. We further demonstrate that nuclear wrinkling can be reversed through osmotic shock and suppressed by microtubule disruption, providing tuneable physical and biological control parameters for probing mechanical properties of the nuclear envelope. Our findings advance the biophysical understanding of nuclear membrane fluctuations during early multicellular development.

Wrinkling and flickering of flexible sheet-like structures essentially determine mechanics and transport in a wide range of physical and biological systems, from graphene [1, 2] and DNA origami [3] to nuclear envelopes (NEs) [4–7] and cell membranes [8, 9]. Over the last decade, much progress has been made through experimental and theoretical work in understanding the effects of environmental fluctuations on the bending behaviors of carbon-based monolayers [10] and the shape deformations of lipid bilayer membranes of vesicles [11–13] and cells [14, 15]. In contrast, the emergence and dynamical evolution of

† dunkel@mit.edu. ‡ jalsous@flatironinstitute.org.
*These authors contributed equally

Author contributions. J.I.A., J.A.J., N.R., J.F.T., J.D., A.C.M. conceived the project. J.I.A., J.A.J. designed and conducted experiments. N.R., K.J.B. and J.F.T. designed and implemented the numerical simulations. N.R. and A.M. performed analytical calculations. J.A.J. and N.R. performed image and data analysis. N.R., J.A.J., J.I.A. and J.D. wrote the original manuscript, with input from all authors. All authors revised the manuscript

Competing interests. The authors declare no competing interests.

Code availability. The code used for numerical simulations is publicly available at https://github.com/NicoRomeo/d3shell.

surface deformations in NEs [6, 7, 16] at different length- and timescales, to which we refer throughout this paper simply as ‘wrinkling’, still pose fundamental open questions, as performing three-dimensional (3D) observations at high spatio-temporal resolution remains challenging under natural physiological and developmental growth conditions. Specifically, it is unclear how NE wrinkle formation proceeds during cellular development, which biophysical processes govern wrinkle morphology, and whether there exist characteristic scaling laws for NE surface fluctuations [5, 6, 17]. Addressing these questions through quantitative measurements promises insights into the physics of complex membranes and can clarify the biological and biomedical implications of NE deformations that have been linked to gene expression [6], cellular aging [18], and diseases like progeria syndrome [4, 19].

Here, we combine 3D confocal microscopy, theoretical analysis, and simulations to characterize the wrinkling morphology and dynamics of nuclear surfaces in fruit fly egg chambers. A spectral analysis of over 300 nuclei provides evidence for an asymptotic power-law scaling of the surface fluctuations, consistent with predictions from renormalization calculations [20, 21] and scaling arguments based on a nonlinear elasticity model for thin shells. Although the scaling is found to be highly robust against physical and biological perturbations, its magnitude (prefactor) can be tuned via osmotic pressure variation and microtubule disruption. These two different control mechanisms enable the tuning and probing of the NE’s spectral and mechanical properties, and provide biophysical strategies for suppressing and reversing nuclear wrinkling.

The NE is a double membrane that separates the cell’s nuclear interior from the surrounding cytoplasm. The two concentric ~4nm-thick lipid bilayers are ~20–50nm apart and are supported by the nuclear lamina, a noncontractile meshwork of intermediate filaments that lie adjacent to the inner nuclear membrane, conferring mechanical stability and affecting essential cellular processes through regulation of chromatin organization and gene expression [22, 23]. Among other proteins, the NE contains nuclear pore complexes, multi-protein channels that primarily regulate passage of macromolecules between the nucleus and the cytoplasm [24, 25]. Recent *in vitro* studies have provided key insights into the role of lamins, cytoplasmic structures, and the physical environment in affecting NE morphology, as well as evidence for the critical importance of nuclear shape for many cellular and nuclear functions [4, 17], including transcriptional dynamics [6]. Despite notable progress, a quantitative understanding of how wrinkling phenomenology and 3D spectral properties of nuclear surfaces evolve in time and during cellular development has remained elusive.

To investigate the biophysical dynamics, scaling behaviors, and reversibility of nuclear wrinkling, we used the egg chamber of the fruit fly *Drosophila melanogaster*, a powerful system amenable to 3D high-resolution live imaging and targeted biological and physical perturbations [26]. The egg chamber contains 15 nurse cells and the oocyte (the immature egg cell), all connected via cytoplasmic bridges and enclosed by a thin layer of hundreds of follicle cells (Fig. 1a, with schematics in Supp. Fig. S1a, [27]). For most of the ~3 days of oogenesis, the nurse cells supply proteins, mRNAs, and organelles to the oocyte through diffusion and microtubule-mediated directed transport [28–31]. To provide the prodigious amount of material and nutrients that the oocyte needs, each nurse cell replicates its DNA

~10 times without undergoing cell division, thereby notably increasing its nuclear and cell sizes [32]. In the ~30-hour window studied here, the diameter of nurse cell nuclei in the cells directly connected to the oocyte increases from approximately 16 to about 40 micrometers [32, 33], accompanied by the progressive appearance of fold-like deformations in the NE, providing an ideal test bed for studying the onset and evolution of NE wrinkling (Fig. 1b,c).

To compare nurse cell nuclei within the same egg chamber and across different egg chambers, we defined a proxy measurement for developmental time (referred to here as the 'time proxy') based on the geometric average of the egg chamber's length and width (Methods, SI Sec. III 1, Supp. Fig. S1b,c). Since egg chamber geometry correlates closely with developmental progression, adopting this continuous geometric characterization offers finer temporal resolution than the traditional approach of distinguishing 14 discrete morphological stages [28, 29] (for a comparison between the time proxy and developmental stage, see Supp. Fig. S1c). By time-ordering nuclei according to this metric, we could more accurately determine the time of emergence of nuclear wrinkling and reconstruct its evolution (Fig. 1b,c). To track the NEs of the nurse cells in space and time, we used a fluorescently-tagged version of the nuclear pore complex protein Nup107 that delineates the nucleus (Supplementary Video 1; qualitatively similar wrinkling patterns were observed using a different labeled protein in the NE and via label-free imaging, see Supp. Fig. S2); note that this label allows observation only of deformations that include both membranes of the nuclear envelope, but is unlikely to label deformations that include only the inner membrane, such as Type I nucleoplasmic reticula [34, 35]. Having acquired highly resolved 3D imaging data (Fig. 1c, Supp. Fig. S3), we reconstructed the nuclear surface radius $R(\theta, \phi)$ relative to the geometric center of the nucleus, where θ and ϕ are the spherical polar angles.

To obtain a compact 3D spectral representation of the nuclear surface deformations, we computed the real spherical harmonic coefficients f_{lm}, defined by

$$R(\theta, \phi) = \sum_{l=0}^{l_{\max}} \sum_{m=-l}^{l} f_{lm} Y_{lm}(\theta, \phi), \tag{1}$$

where Y_{lm} is the spherical harmonic with angular number l and order m (Methods). Equation (1) allows for a continuous reconstruction of the NEs (Fig 1d, Supp. Fig. S3), with the mode-cutoff $l_{\max}$ setting the angular resolution of the spectral representation (Methods). The coefficient values $\{f_{lm}\}$ depend on the choice of coordinate system, that is, the orientation of the nuclei. To obtain a rotation-invariant characterization of the surface wrinkles, we consider the power spectrum of radial out-of-plane deformations

$$P_l = \frac{4\pi}{(2l+1) f_{00}^2} \sum_{m=-l}^{l} f_{lm}^2, \tag{2}$$

normalized by the average radius of the shell $\langle R \rangle = f_{00}/\sqrt{4\pi}$. The non-negative numbers P_l measure the average power in a mode of angular wavenumber l. A single-valued summary statistic of surface wrinkling can be given in terms of the 'roughness' parameter $\mathscr{R} = \sum_{l \geq 3}(2l+1)P_l$, the total power contained in angular numbers $l \geq 3$. By ignoring the long-wavelength modes $l < 3$, $\mathscr{R}$ measures the contribution of finer-scale wrinkles to NE deformations. Our analysis of over 300 nurse cell nuclei shows that the power spectrum of NEs maintains an approximately constant shape as development progresses, but with a steadily-increasing amplitude (Fig. 1e; Supp. Fig. S4), reflecting the fact that wrinkling becomes more pronounced as nuclei increase in size. $\mathscr{R}$ increases exponentially with the time proxy (Fig. 1f), suggesting that nurse cell nuclei transition smoothly from an unwrinkled to a wrinkled state.

Nuclear surface wrinkling is a highly dynamic process [6]. By imaging individual nurse cells at ~40 s intervals, we too observed that NE surface shapes fluctuate substantially, with smaller features appearing and disappearing faster than larger ones (Fig. 1g, Supplementary Video 2). Specifically, power spectra P_l of repeatedly imaged nuclei changed on timescales of minutes or faster (Supp. Fig. S4 and Supp. Fig. S5). The rotational invariance of spectra implies that these fluctuations are not the result of whole body rotations, but instead reflect a rapid shape dynamics of NE surfaces. Experimental limitations prevented quantification of timescales for the entire 3D surface, but our observations are qualitatively consistent with findings that smaller wrinkles typically decay faster [15, 36]. Furthermore, the fact that the deformation spectrum is monotonically decreasing (Fig. 1e) implies that there is no preferred wavelength, suggesting that the observed NE shapes do not correspond to fluctuations about the steady-states of buckled shells, but instead reflect dynamic wrinkling across all experimentally resolved angular scales.

Both maximum-intensity projections and spectral reconstructions show that NE wrinkles and creases are sharp, with narrow bent regions separated by flatter areas (Fig. 1). This morphology is reminiscent of the nonlinear stress-focusing characteristic of crumpled elastic sheets and shells such as ordinary paper sheets, which are much more easily bent than stretched [1, 37, 38]. In particular, these geometric nonlinearities lead to anisotropic responses when point forces are applied to the shell [38]. To rationalize the experimentally observed wrinkle morphology at spatial scales larger than the NE thickness, we constructed a minimal effective elastic model, describing the NE as a deformed spherical shell (equilibrium radius R). In spherical coordinates $\mathbf{r} = (\theta, \phi)$, the shell has an isotropic elastic free energy [21, 39]

$$F_{\text{shell}} = \int \mathrm{d}^2\mathbf{r}\left[\frac{\kappa}{2}\left(\nabla^2 f\right)^2 + \frac{\lambda}{2}\epsilon_{ii}^2 + \mu\epsilon_{ij}^2\right], \tag{3}$$

where $i, j \in \{\theta, \phi\}$ and using the Einstein summation convention. The energy functional (3), accounts for bending stiffness through a Helfrich-like bending term that penalizes out-of-plane deformation f (positive when pointing inwards), and the stretching of the membrane through the nonlinear strain tensor ϵ_{ij}. The 2D Lamé parameters λ, μ are proportional to the

2D Young's modulus Y. The strain combines contributions from f and from the in-plane deformation $\mathbf{u}(\mathbf{r})$ (SI Sec. IV). We also allow for a preferred radius of curvature R_c of the shell mismatched with the radius R of the shell $R_c \geq R$, which in the large-Föppl-von Kármán (FvK) regime leads to a strain tensor $\epsilon_{ij} = \frac{1}{2}(\partial_i u_j + \partial_j u_i + \partial_i f \partial_j f) - \delta_{ij} f / R_c$ (SI Sec. IV). Previous work [40–42] has shown the NE to be stiffer than most biological membranes and to be well described as a thin membrane of a 3D isotropic elastic material with an effective 3D Young's modulus $E \approx 1$ kPa and thickness of $h \sim 10 - 100$ nm (for a more detailed discussion of limitations of fluid membrane models, see SI Sec. IV 5), leading to a bending rigidity of $\kappa = 100 - 300\, kT_{eq} \approx 10^{-18}$ J, where T_{eq} is the room temperature, and a stretching rigidity, captured by the 2D Young's modulus, of $Y \approx 10^{-4}$ N/m [43]. By construction, these moduli are approximately related through the effective thickness $h \sim \sqrt{\kappa / Y}$ [21]. Note that Y is a factor of 10^3 smaller than the stretching rigidity of a lipid bilayer, potentially explained by the presence of 'area reservoirs' in NEs and by transmembrane protein conformational changes [44]. For a shell of radius R, one can define the FvK number $\gamma = YR^2/\kappa$ which describes the relative propensity of the material to bend rather than to stretch. Using the above values, we find that the NE has a large FvK number $\gamma \sim 10^4 - 10^6$, comparable to that of a sheet of paper or graphene [1]. Accordingly, the NE is more amenable to bending than to stretching, and deformations are expected to appear as sharp wrinkles and creases, in agreement with our observations (Fig. 1).

To compare the surface shapes and fluctuation predicted by Eq. (3) with our experimental data, we simulated the equilibrium Langevin PDE derived from this free energy (see Methods and SI Sec. IV 4 for simulation details). The simulations account for hydrodynamic coupling and both passive and active fluctuations, which are modeled by an effective temperature kT_{eff}. Despite the model's minimal character and theoretical limitations of Eq. (3) at long wavelengths where $l \to 0$ (SI Sec. IV), the numerically obtained shapes (Fig. 2a) are qualitatively similar to those in the experiments (Fig. 1d). In the experimentally accessible range of low-to-intermediate angular wave numbers $3 \lesssim l \lesssim 11$, the angular spectra extracted from the simulations at different ratios of $kT_{eff}/\kappa \in [0.05,\ 0.5]$ (Fig. 2b) and experimental data (Fig. 1e) also show an approximately similar decay, suggesting that the minimal elastic shell model in Eq. (3) captures relevant features of the NE, providing a basis for further analysis and predictions.

A main feature of the experimentally measured spectra is that both younger and older nuclei exhibit a similar asymptotic power law decay in the limit of small angular numbers $l \leq 10$ (Fig. 2c). To rationalize this observation, we first note that the scaling behavior in our experiments deviates from the basic linear response theory predictions, which is expected because, even for younger nuclei, the radial fluctuations f typically exceed the NE thickness $h \sim 10^{-3} R$ (Fig. 1c–f). More precisely, for small fluctuations ($f \ll h \ll R$) and small thermodynamic pressure $\left(p \ll p_c = 4\sqrt{\kappa Y}/R_c^2\right.$, where p_c is the critical buckling pressure of the sphere), linear response theory predicts that the power spectrum P_l exhibits a plateau for $l \leq l_c$ and falls of as l^{-4} for $l \gg l_c$ with a crossover value $l_c \approx \gamma^{1/4}\sqrt{R/R_c}$ (SI Sec. IV) [21, 45], which is not seen in our experiments (Figs. 1e and 2c). Indeed, classical shell theory

[2] states that nonlinear effects become important when the out-of-plane deformations f become comparable to or exceed the shell thickness h, which is generally the case in our data where $h \ll f \ll R$ (Fig. 1c,d,g). Nonlinear analysis of elastic plates and shells has a long history [20, 46] and has seen major advances in the last decade [21, 39], motivated in part by the discovery of graphene [47]. As demonstrated above, the FvK number of the NE is comparable to that of graphene, so we can borrow and apply recent theoretical results to understand the fluctuation spectra of the NE. Specifically, a detailed renormalization group (RG) analysis [21, 48] of Eq. (3) showed that, for sufficiently small plate fluctuations, elastic nonlinearities lead to a modified asymptotic decay of $P_l \propto l^{-3.2}$, consistent with our experimental and simulated data (Figs. 1e and 2b,c) and with previous experiments in red blood cell spectrin networks [49]. Notably, earlier studies [20, 21, 39] also predicted that the interplay of elastic nonlinearities and fluctuations can cause the spontaneous collapse of sufficiently large shells, suggesting a physical mechanism that could contribute to the eventual breakdown of the nurse cell NE when these cells donate their contents to the oocyte [30, 50].

The previously mentioned RG methods can give rise to divergences in large deformation regimes, where nonlinearities dominate the shell's response (SI Sec. IV, Fig. S9). To obtain an analytical prediction for the scaling in the larger-deformation regime $h \ll f \ll R < R_c$, relevant to older nuclei, we performed an asymptotic dimensional analysis that provides additional insight into how NE wrinkling can be controlled. To that end, we added to the elastic free energy F_{shell} an effective pressure term $F_p = -\int \mathrm{d}^2\mathbf{r} p_{\text{eff}} f$, where p_{eff} accounts for a normal load, which may arise from osmotic pressure differences or microtubule-induced local stresses. Denoting by L the characteristic surface variation length scale and omitting numerical prefactors that depend on details of the adopted thin-shell modeling approach (SI Sec. IV), one finds for shells of thickness $h \sim \sqrt{\kappa/Y}$ that the various free-energy components give scaling contributions of the form [21]

$$\frac{\delta F}{Y} \sim \left(\frac{h}{L}\right)^2 \left(\frac{f}{L}\right)^2 + \left(\frac{f}{R_c}\right)^2 + \frac{f}{R_c}\left(\frac{f}{L}\right)^2 + \left(\frac{f}{L}\right)^4 - \frac{p_{\text{eff}} f}{Y}. \tag{4}$$

The first term corresponds to bending, and the second and third terms arise from the non-zero curvature of the undeformed shell. The fourth term describes the nonlinear response associated with changes in the Gaussian curvature of the shells. For well-developed wrinkles with $f \gg h$, the first term can be neglected as it is smaller than the fourth term. Considering wrinkle amplitudes f_l at the spatial length scale $L \sim R/l$, where l is the angular wave number, the remaining terms can be recast as

$$\frac{\delta F_l}{Y} \sim \left(\frac{f_l}{R_c}\right)^2 + \frac{f_l}{R_c}\left(\frac{f_l}{R}\right)^2 l^2 + \left(\frac{f_l}{R}\right)^4 l^4 - \frac{p_{\text{eff}}}{Y} f_l. \tag{5}$$

Since $R_c > R$, the first two terms will be dominated by the l^4-term implying that, at steady-state, this quartic term and the pressure term must balance out, consistent with a corresponding earlier result for flat plates with $R_c = \infty$ [2]. We thus find $f_l \sim (p_{\text{eff}}/Y)^{1/3}(R/l)^{4/3}$, and hence for the angular power spectrum $P_l \sim (f_l/R)^2$ [see Eq. (2)] the scaling law

$$P_l \sim \left(\frac{p_{\text{eff}} R}{Y}\right)^{2/3} l^{-8/3}. \tag{6}$$

In this scaling regime, the surface deformation dynamics is dominated by the shell's resistance to stretching, which causes changes in its Gaussian curvature [51]. Both our experimental data (Fig. 2c, Supp. Fig. S4) and spherical shell simulations (SI, Supp. Fig. S8) show an asymptotic spectral decay $P_l \propto l^{-\alpha}$ with an exponent α in the range $8/3 < \alpha < 3.2$, predicted by this scaling analysis and renormalization group calculations.

Both Eq. (6) and the robustness of the experimentally observed scaling behavior in time (Fig. 2c, Supp. Fig. S4), and under different chemical and physical perturbations (Fig. 3), suggest the emergence of NE wrinkling is primarily controlled by the material properties and the effective pressure p_{eff} induced by thermal and by active fluctuations. For Gaussian fluctuations with effective temperature T_{eff}, previous theoretical work [21,39] showed that $p_{\text{eff}} \sim p_c(kT_{\text{eff}})\sqrt{\gamma} \sim (Y/R)(kT_{\text{eff}}/\kappa)$, with $p_c = 4\sqrt{\kappa Y}/R^2$ the critical buckling pressure for a homogeneous spherical shell. If in addition to a fluctuating pressure p', there are uniform loads, such as those caused by osmotic pressure differences, we find $p_{\text{eff}} = p'(R/\langle R \rangle)^3$ accounts for excess area contributions to the amplitude (as long as the shell is not stretched taut; SI Sec. IV 3). Inserting these results into Eq. (6), scaling analysis predicts that wrinkle formation can be tuned by changing the bending rigidity κ, the activity kT_{eff} and the cell's osmotic pressure balance (for comparison with RG predictions, see SI Sec. IV 2 2.4).

To test these predictions and investigate the role of the NE's material structure during wrinkle formation, we performed live-imaging experiments in which we measured the concentration of a structural component that determines nuclear stiffness. Elastic properties of the NE are known to depend strongly on the nuclear lamina [52], a roughly 10–100 nm thick meshwork of intermediate filaments that abuts the NE's inner membrane [22]. *Drosophila* have two lamin proteins, Lamin C (a developmentally-regulated A-type lamin similar to mammalian Lamin A/C, [53, 54]) and Lamin Dm0 (a B-type lamin present in most cell types). Both through live imaging of egg chambers simultaneously expressing a fluorescently-labeled nuclear pore complex protein (Nup107) and Lamin C, and through fixed imaging with an antibody against Lamin C, we found that, as egg chambers age and nurse cells grow in size, the ratio of Lamin C to Nup107 decreases (Fig. 2d,e; Supp. Fig. S6a–c) while the intensity of Nup107 remains roughly constant (Supp. Fig. S6d). Nonetheless, at the spatial scales resolved experimentally, Lamin C continues to appear alongside Nup107 at the sites of wrinkles (Supp. Fig. S6ei). This reduction in Lamin C concentration might cause softening of the NE and a reduced bending rigidity κ that increases wrinkle amplitudes [52] as predicted by Eq. (6). However, given the challenge in

performing perturbative studies (see Discussion and SI Sec. I6), it is not possible to assess the functional importance of Lamin C decrease from our data.

In addition to material properties, active fluctuations [55] or hydrodynamic effects [11, 56] can substantially affect buckling and pattern formation in shells and membranes [12, 57, 58]. To explore how changes in cytoskeleton-mediated intracellular activity [59] influence the spectrum of NE deformation, we performed additional perturbation experiments targeting the cytoplasmic microtubule and actin networks. Previous work showed that incoherent microtubule dynamics can cause fluctuations of the NE during cellularization of the *Drosophila* embryo [60]. Consistent with this earlier report and with the predictions of Eq. (6), we found that inhibition of microtubule polymerization by the small-molecule inhibitor colchicine notably reduces the amplitude of fluctuations (Fig. 3a; Supp. Fig. S11a,b; Supplementary Videos 4,5). Colchicine treatment also decreased nucleus volume by 5%–20%; however, as a volume decrease for a similar surface area would lead to a rougher rather than a smoother NE in the absence of other factors, it is unlikely that volume reduction explains the effects seen upon colchicine treatment. Furthermore, colchicine addition reduced the motion of cytoplasmic contents of the cells (Supplementary Videos 6,7), suggesting microtubule-mediated active fluctuations contribute to NE wrinkling. However, colchicine addition in older egg chambers (time proxies roughly over 185) had a less noticeable effect, decreasing rotational motion of the nuclei but not leading to the same extent of observable unwrinkling as in younger egg chambers. In contrast, perturbation of actin by cytochalasin D did not unwrinkle the NE (Supp. Fig. S11c,d; Supplementary Videos 8,9), suggesting cytoplasmic F-actin is not a major contributor to NE wrinkling during the developmental stages studied here. The observation that inhibition of microtubule polymerization reduces the wrinkle amplitude but does not change the spectral scaling behavior (Fig. 3d) suggests that, to leading order, non-equilibrium contributions to NE fluctuations arising from microtubule dynamics can be modeled through an effective temperature kT_{eff} [9, 15]. We also tested other mechanisms known to contribute to NE deformation, such as sustained impingement by cytoskeletal filaments or changes to chromatin structure (SI Sec. II), but found Lamin C decrease to be the dominant factor correlating with NE wrinkle formation (Supp. Fig. S10, S11, S12; Supplementary Video 3). Nonetheless, other factors than the ones addressed in this study could also participate in NE wrinkling, as our model is a simplification of a complex biological process.

Eq. (6) also suggests that osmotic pressure variations can, by tuning the available excess area [61, 62], enhance or reverse wrinkle formation by up- or down-shifting the deformation spectrum without changing its characteristic decay. To test this prediction, we performed osmotic shock experiments and found that adding salt to the ambient culture medium (hypertonic shock) increases the total external pressure on the NE, which drives fluid out of the nucleus and leads to visibly more wrinkled surfaces (Fig. 3b,e). Conversely, reducing the salt concentration in the culture medium (hypotonic shock) decreases the external pressure and leads to substantial smoothening of wrinkled NE (Fig. 3c,e, Supp. Fig. S7; see SI Sec. I 5 for experimental details and SI Sec. IV 3 for an explanation of the connection between osmotic pressure and wrinkle amplitude). In both cases, NEs maintained their altered morphology for 15–30 minutes before nuclear shapes trended back towards their

pre-shock state, presumably through regulatory mechanisms that partially compensate for osmotic changes. In agreement with Eq. (6), the spectral slopes remained approximately preserved for both types of shocks. Taken together, these results support the hypothesis that wrinkle morphology and dynamics of deformation of the nurse cells' NE are dominated by a nonlinear elastic response rather than liquid-like behavior.

NE wrinkles have been associated with biological processes including nuclear positioning [6], and as a mechano-sensitive element of the cell, the NE can regulate chromatin dynamics and force-induced transcription factor movement through nuclear pore complexes [16, 63–65]. Here we observed an increase in NE wrinkling during egg chamber growth that correlates with an increase in nuclear size along with a decay in Lamin C concentrations. Although NE wrinkling may affect the nurse cells' chromatin organization and transcriptional states, NE wrinkles may instead simply result from concomitant nucleus growth and Lamin C density decrease in cells that are fated to die to enable egg development. It is nonetheless tempting to propose that NE wrinkles could act as a tension buffer: tension applied to the NE would initially unfold the wrinkles before leading to significant in-plane strain that might cause NE rupture. Such a two-stage response to tension has indeed been observed during cell spreading, in which a NE stretch-mediated response occurs only after the initially-wrinkled nucleus flattens by a certain amount [5, 17].

Prior work has shown that some nurse cells in stage 5–9 egg chambers have a high level of intranuclear actin, which decreases from stage 10 onwards [66]. Additionally, in other contexts such as the *Drosophila* larval muscle, Lamin C mutants can induce formation of intranuclear actin rods and potentially deform the nuclei [67]. These findings suggest that changes in intranuclear actin levels or organization may also affect wrinkling; however, whether they increase or decrease wrinkling remains unclear (see SI Sec. II). Another future prospect is to investigate how NE wrinkling changes when Lamin C density is exogenously modified, allowing further comparisons to theory and clarifying whether NE wrinkling has biological function. Due to complications with existing fly reagents for perturbing Lamin C levels in the female germline, increasing or decreasing expression of Lamin C in the nurse cell NEs proved challenging (see SI Sec. I 6 for details); therefore, developing such genetic tools would constitute a substantial technical advance. A further limitation of our study is that the continuum model is a simplification of the complex anatomy of the NE and that our measurements cannot distinguish between features that only include a single NE membrane layer or are below the resolution limit of confocal light microscopy.

To conclude, our experimental and theoretical results suggest that essential qualitative aspects of NE wrinkling can be understood within the framework of nonlinear elastic thin-shell mechanics. As NEs have a Föpplvon Kármán number similar to both graphene and paper [1], we expect our theoretical observations to be relevant for these and other similar systems, where fluctuations push the membranes and shells into larger deformation regimes. With the power-law exponent set by the elastic behavior of the shell, the amplitude of wrinkles is controlled by the effective pressure, which we have manipulated here through osmotic shocks and microtubule inhibition. Our findings therefore raise the question of whether cellular control over pressure could be a generic biophysical mechanism for avoiding undesirable consequences of NE wrinkling [4, 17, 19].

1. METHODS

Detailed descriptions of experimental methods, image processing, simulations, and theory can be found in the Supplementary Information.

A. Experiments

A list of fly lines used for this study can be found in Table S1. In short, ovaries were removed from well-fed flies and cultured *ex vivo* [68] for 1–4 hours. Images were acquired using laser-scanning confocal microscopy with a 40x/1.2NA water or 63x/1.4NA oil objective. For immunofluorescence, ovaries were fixed in 4% (wt/vol) paraformaldehyde and stained with phalloidinAlexa-568, Hoechst, and antibodies against Lamin C or tri-methylated histone H3K9. Perturbations were performed by adding NaCl-spiked culture medium, water, or small-molecule inhibitors to the culture medium to the following final conditions: 1.5x original osmolarity (hypertonic shock), 0.5x osmolarity (hypotonic shock), 9mg/mL colchicine, or 10 μg/mL cytochalasin D.

B. Image processing

Nuclear envelopes were segmented and their coordinates extracted using FIJI and the MorphoLibJ plugin [69, 70]. Custom-built Matlab code [71] was used to perform least-square fits to determine spherical harmonic coefficients up-to the cutoff mode number $l_{\max} = 25$, which corresponds to an angular scale of roughly 7°, as well as to measure the LamC:Nup107 ratio over developmental time.

C. Simulations

We use the pseudo-spectral solver Dedalus 3 [72] to solve the Langevin equation derived from the non-euclidean elastic free energy Eq. (3) accounting for hydrodynamic interactions with a viscous environment [15, 73]; see the Supplementary Information for details and validations. Due to the stiffness of the equations governing the dynamics of plates and shells, simulations of such thin surfaces is numerically expensive. We simulate the partial differential equations on a 512 × 256 Driscoll-Healy spherical coordinate grid, for 3×10^5 timesteps using the MIT Supercloud cluster [74]. Each simulation is run on 32 cores for a total of approximately ~360 hours of CPU time per simulation. Additional processing to study simulation results used the pyshtools library [75]. The fact that the power spectrum P_l does not change qualitatively when the nuclear radius R increases suggests that the preferred curvature radius R_c is rather large. In simulations, we thus set the preferred curvature radius to $R_c = 20R$ (SI Sec. IV 4). Consistent with experiments (Fig. 2c), the appearance of a plateau region in the power spectrum P_l at small angular numbers is suppressed for this choice of R_c (SI Sec. IV 22.1, Suppl. Fig. S8). Indeed, the typical length scale above which finite-curvature effects become visible is $L_{\mathrm{el}} = R\gamma^{-1/4}\sqrt{R_c/R}$, which is for FvK number $\gamma = 10^4$ and $R_c = 20R$ approximately equal to $R/2$. Further details on parameter selections are provided in SI Sec. IV 4.

Supplementary Material

Refer to Web version on PubMed Central for supplementary material.

Acknowledgments

The authors thank the MIT SuperCloud and Lincoln Laboratory Supercomputing Center for providing HPC resources that have contributed to the research results reported within this paper. We thank Mehran Kardar, Roger D. Kamm, Eric Folker, Mary Ann Collins and Douglas P. Holmes for helpful discussions. This work was supported by a MathWorks Science Fellowship (N.R.), NSF Award DMS-1952706 (J.D. and N.R.), Sloan Foundation Grant G-2021-16758 (J.D.), MIT Mathematics Robert E. Collins Distinguished Scholar Fund (J.D.), Feodor Lynen Research Fellowship from the Humboldt foundation (J.F.T.), Jarve Fund MIT grant (A.C.M. and J.D.), and the National Institute of General Medical Sciences of the National Institutes of Health under award number R01GM144115 (A.C.M). N.R. and J.F.T. acknowledge participation in the KITP online workshop 'The Physics of Elastic Films: from Biological Membranes to Extreme Mechanics' supported in part by the National Science Foundation under Grant No. NSF PHY-1748958.

Data availability.

All data supporting the findings of this work are available within the manuscript and Supplementary Information files. Higher-resolution images, point cloud data, spherical harmonic processing codes and spreadsheets containing the experimental data points shown in plots are available on figshare 10.6084/m9.figshare.23800287 Raw microscopy data is available upon request due to file size limitations.

References

[1]. Blees Melina K., Barnard Arthur W., Rose Peter A., Roberts Samantha P., McGill Kathryn L., Huang Pinshane Y., Ruyack Alexander R., Kevek Joshua W., Kobrin Bryce, Muller David A., and McEuen Paul L.. Graphene kirigami. Nature, 524(7564):204–207, August 2015. [PubMed: 26222025]

[2]. Los JH, Fasolino A, and Katsnelson MI. Mechanics of thermally fluctuating membranes. npj 2D Materials and Applications, 1(1):9, December 2017.

[3]. Yoo Jejoong and Aksimentiev Aleksei. In situ structure and dynamics of DNA origami determined through molecular dynamics simulations. Proceedings of the National Academy of Sciences, 110(50):20099–20104, December 2013.

[4]. Kalukula Yohalie, Stephens Andrew D., Lammerding Jan, and Gabriele Sylvain. Mechanics and functional consequences of nuclear deformations. Nature Reviews Molecular Cell Biology, 23(9):583–602, September 2022. [PubMed: 35513718]

[5]. Lomakin AJ, Cattin CJ, Cuvelier D, Alraies Z, Molina M, Nader GPF, Srivastava N, Sáez PJ, Garcia-Arcos JM, Zhitnyak IY, Bhargava A, Driscoll MK, Welf ES, Fiolka R, Petrie RJ, De Silva NS, González-Granado JM, Manel N, Lennon-Duménil AM, Müller DJ, and Piel M. The nucleus acts as a ruler tailoring cell responses to spatial constraints. Science, 370(6514):eaba2894, October 2020. [PubMed: 33060332]

[6]. Almonacid Maria, Jord Adel Al, El-Hayek Stephany, Othmani Alice, Coulpier Fanny, Lemoine Sophie, Miyamoto Kei, Grosse Robert, Klein Christophe, Piolot Tristan, Mailly Philippe, Voituriez Raphaël, Genovesio Auguste, and Verlhac Marie-Hélène. Active Fluctuations of the Nuclear Envelope Shape the Transcriptional Dynamics in Oocytes. Developmental Cell, 51(2):145–157.e10, October 2019. [PubMed: 31607652]

[7]. Biedzinski Stefan, Agsu Gökçe, Vianay Benoit, Delord Marc, Blanchoin Laurent, Larghero Jerome, Faivre Lionel, Théry Manuel, and Brunet Stéphane. Microtubules control nuclear shape and gene expression during early stages of hematopoietic differentiation. The EMBO Journal, 39(23):e103957, 2020. [PubMed: 33089509]

[8]. Brochard F and Lennon JF. Frequency spectrum of the flicker phenomenon in erythrocytes. Journal de Physique, 36(11):1035–1047, 1975.

[9]. Betz Timo, Lenz Martin, Joanny Jean-François, and Sykes Cécile. ATP-dependent mechanics of red blood cells. Proceedings of the National Academy of Sciences, 106(36):15320–15325, September 2009.

[10]. Bowick Mark J., Andrej Košmrlj David R. Nelson, and Sknepnek Rastko. Non-Hookean statistical mechanics of clamped graphene ribbons. Physical Review B, 95(10):104109, March 2017.

[11]. Kantsler Vasiliy, Segre Enrico, and Steinberg Victor. Vesicle Dynamics in Time-Dependent Elongation Flow: Wrinkling Instability. Physical Review Letters, 99(17):178102, October 2007. [PubMed: 17995373]

[12]. Kokot Gašper, Faizi Hammad A., Pradillo Gerardo E., Snezhko Alexey, and Vlahovska Petia M.. Spontaneous self-propulsion and nonequilibrium shape fluctuations of a droplet enclosing active particles. Communications Physics, 5(1):91, December 2022.

[13]. Honerkamp-Smith Aurelia R., Woodhouse Francis G., Kantsler Vasily, and Goldstein Raymond E.. Membrane viscosity determined from shear-driven flow in giant vesicles. Phys. Rev. Lett, 111:038103, Jul 2013. [PubMed: 23909365]

[14]. Eyal Ben-Isaac YongKeun Park, Popescu Gabriel, Brown Frank L. H., Gov Nir S., and Shokef Yair. Effective Temperature of Red-Blood-Cell Membrane Fluctuations. Physical Review Letters, 106(23):238103, June 2011. [PubMed: 21770546]

[15]. Turlier H, Fedosov DA, Audoly B, Auth T, Gov NS, Sykes C, Joanny J-F, Gompper G, and Betz T. Equilibrium physics breakdown reveals the active nature of red blood cell flickering. Nature Physics, 12(5):513–519, May 2016.

[16]. Chu Fang-Yi, Haley Shannon C., and Zidovska Alexandra. On the origin of shape fluctuations of the cell nucleus. Proceedings of the National Academy of Sciences, 114(39):10338–10343, September 2017.

[17]. Venturini Valeria, Pezzano Fabio, Castro Frederic Català, Häkkinen Hanna-Maria, Jiménez-Delgado Senda, Colomer-Rosell Mariona, Marro Monica, TolosaRamon Queralt, Paz-López Sonia, Valverde Miguel A., Weghuber Julian, Loza-Alvarez Pablo, Krieg Michael, Wieser Stefan, and Ruprecht Verena. The nucleus measures shape changes for cellular proprioception to control dynamic cell behavior. Science, 370(6514):eaba2644, October 2020. [PubMed: 33060331]

[18]. di Paola Sca and Misteli Tom. Lamin A-Dependent Nuclear Defects in Human Aging. Science, 312(5776):1059–1063, May 2006. [PubMed: 16645051]

[19]. Mounkes Leslie C., Kozlov Serguei, Hernandez Lidia, Sullivan Teresa, and Stewart Colin L.. A progeroid syndrome in mice is caused by defects in A-type lamins. Nature, 423(6937):298–301, May 2003. [PubMed: 12748643]

[20]. Nelson D, Piran T, and Weinberg S. Statistical Mechanics of Membranes and Surfaces: Proceedings of the Jerusalem Winter School for Theoretical Physics. World Scientific, Jerusalem, Israel, April 1989.

[21]. Košmrlj Andrej and Nelson David R.. Statistical Mechanics of Thin Spherical Shells. Physical Review X, 7(1):011002, January 2017.

[22]. Aebi Ueli, Cohn Julie, Buhle Loren, and Gerace Larry. The nuclear lamina is a meshwork of intermediate-type filaments. Nature, 323(6088):560–564, October 1986. [PubMed: 3762708]

[23]. Lammerding Jan, Schulze P. Christian, Takahashi Tomosaburo, Kozlov Serguei, Sullivan Teresa, Kamm Roger D., Stewart Colin L., and Lee Richard T.. Lamin A/C deficiency causes defective nuclear mechanics and mechanotransduction. Journal of Clinical Investigation, 113(3):370–378, February 2004. [PubMed: 14755334]

[24]. Strambio-De-Castillia Caterina, Niepel Mario, and Rout Michael P.. The nuclear pore complex: bridging nuclear transport and gene regulation. Nature Reviews Molecular Cell Biology, 11(7):490–501, July 2010. [PubMed: 20571586]

[25]. Knockenhauer Kevin E. and Schwartz Thomas U.. The Nuclear Pore Complex as a Flexible and Dynamic Gate. Cell, 164(6):1162–1171, March 2016. [PubMed: 26967283]

[26]. Hudson Andrew M. and Cooley Lynn. Methods for studying oogenesis. Methods, 68(1):207–217, June 2014. [PubMed: 24440745]

[27]. King RC, Rubinson AC, and Smith RF. Oogenesis in adult Drosophila melanogaster. Growth, 20(2):121–157, June 1956. [PubMed: 13366067]

[28]. McLaughlin John M. and Bratu Diana P.. Drosophila melanogaster Oogenesis: An Overview. In Bratu Diana P. and McNeil Gerard P., editors, Drosophila Oogenesis, volume 1328, pages 1–20. Springer New York, New York, NY, 2015. Series Title: Methods in Molecular Biology.

[29]. Bastock Rebecca and Johnston Daniel St. Drosophila oogenesis. Current Biology, 18(23):R1082–R1087, December 2008. [PubMed: 19081037]

[30]. Jasmin Imran Alsous Nicolas Romeo, Jackson Jonathan A., Mason Frank M., Dunkel Jörn, and Martin Adam C.. Dynamics of hydraulic and contractile wave-mediated fluid transport during *Drosophila* oogenesis. Proceedings of the National Academy of Sciences, 118(10):e2019749118, March 2021.

[31]. Mahajan-Miklos Shalina and Cooley Lynn. Intercellular Cytoplasm Transport during Drosophila Oogenesis. Developmental Biology, 165(2):336–351, October 1994. [PubMed: 7958404]

[32]. Lin Haifan and Spradling Allan C.. Germline Stem Cell Division and Egg Chamber Development in Transplanted Drosophila Germaria. Developmental Biology, 159(1):140–152, September 1993. [PubMed: 8365558]

[33]. Tzur Amit, Kafri Ran, LeBleu Valerie S., Lahav Galit, and Kirschner Marc W.. Cell Growth and Size Homeostasis in Proliferating Animal Cells. Science, 325(5937):167–171, July 2009. [PubMed: 19589995]

[34]. Malhas Ashraf N. and Vaux David J.. Nuclear Envelope Invaginations and Cancer, pages 523–535. Springer New York, New York, NY, 2014.

[35]. Fricker Mark, Hollinshead Michael, White Nick, and Vaux David. Interphase Nuclei of Many Mammalian Cell Types Contain Deep, Dynamic, Tubular Membrane-bound Invaginations of the Nuclear Envelope. Journal of Cell Biology, 136(3):531–544, February 1997. [PubMed: 9024685]

[36]. Zilman AG and Granek R. Undulations and Dynamic Structure Factor of Membranes. Physical Review Letters, 77(23):4788–4791, December 1996. [PubMed: 10062631]

[37]. Andrejevic Jovana, Lee Lisa M., Rubinstein Shmuel M., and Rycroft Chris H.. A model for the fragmentation kinetics of crumpled thin sheets. Nature Communications, 12(1):1470, December 2021.

[38]. Witten TA. Stress focusing in elastic sheets. Reviews of Modern Physics, 79(2):643–675, April 2007.

[39]. Paulose J, Vliegenthart GA, Gompper G, and Nelson DR. Fluctuating shells under pressure. Proceedings of the National Academy of Sciences, 109(48):19551–19556, November 2012.

[40]. Guilak Farshid, Tedrow John R., and Burgkart Rainer. Viscoelastic Properties of the Cell Nucleus. Biochemical and Biophysical Research Communications, 269(3):781–786, March 2000. [PubMed: 10720492]

[41]. Funkhouser Chloe M., Sknepnek Rastko, Shimi Takeshi, Goldman Anne E., Goldman Robert D., and Monica Olvera de la Cruz. Mechanical model of blebbing in nuclear lamin meshworks. Proceedings of the National Academy of Sciences, 110(9):3248–3253, February 2013.

[42]. Kim Dong-Hwee, Li Bo, Si Fangwei, Phillip Jude M., Wirtz Denis, and Sun Sean X.. Volume regulation and shape bifurcation in the cell nucleus. Journal of Cell Science, 128(18):3375–3385, September 2015. [PubMed: 26243474]

[43]. Kris Noel Dahl Samuel M. Kahn, Wilson Katherine L., and Discher Dennis E.. The nuclear envelope lamina network has elasticity and a compressibility limit suggestive of a molecular shock absorber. Journal of Cell Science, 117(20):4779–4786, September 2004. [PubMed: 15331638]

[44]. Enyedi Balázs and Niethammer Philipp. Nuclear membrane stretch and its role in mechanotransduction. Nucleus, 8(2):156–161, March 2017. [PubMed: 28112995]

[45]. Pécréaux J, Döbereiner H-G, Prost J, Joanny J-F, and Bassereau P. Refined contour analysis of giant unilamellar vesicles. The European Physical Journal E, 13(3):277–290, March 2004.

[46]. Landau Lev Davidovitch, Lifshitz Evgenij M., Landau Lev Davidovitch, and Landau Lev Davidovitch. Theory of elasticity. Number 7 in Course of theoretical physics / Landau LD and Lifshitz EM. Elsevier, Butterworth-Heinemann, Amsterdam Heidelberg, 3. engl. ed., rev. and enlarged, [nachdr.] edition, 2009.

[47]. Novoselov KS, Geim AK, Morozov SV, Jiang D, Zhang Y, Dubonos SV, Grigorieva IV, and Firsov AA. Electric Field Effect in Atomically Thin Carbon Films. Science, 306(5696):666–669, October 2004. [PubMed: 15499015]

[48]. Baumgarten Lorenz and Kierfeld Jan. Buckling of thermally fluctuating spherical shells: Parameter renormalization and thermally activated barrier crossing. Physical Review E, 97(5):052801, May 2018. [PubMed: 29906947]

[49]. Schmidt Christoph F., Svoboda Karel, Lei Ning, Petsche Irena B., Berman Lonny E., Safinya Cyrus R., and Grest Gary S.. Existence of a Flat Phase in Red Cell Membrane Skeletons. Science, 259(5097):952–955, February 1993. [PubMed: 8438153]

[50]. Yalonetskaya Alla, Mondragon Albert A., Hintze Zackary J., Holmes Susan, and Kimberly McCall. Nuclear degradation dynamics in a nonapoptotic programmed cell death. Cell Death & Differentiation, 27(2):711–724, February 2020. [PubMed: 31285547]

[51]. Gustavo Düring Christophe Josserand, Krstulovic Giorgio, and Rica Sergio. Strong turbulence for vibrating plates: Emergence of a Kolmogorov spectrum. Physical Review Fluids, 4(6):064804, June 2019.

[52]. Swift Joe, Ivanovska Irena L., Buxboim Amnon, Harada Takamasa, Dingal P. C. Dave P., Pinter Joel, Pajerowski J. David, Spinler Kyle R., Shin Jae-Won, Tewari Manorama, Rehfeldt Florian, Speicher David W., and Discher Dennis E.. Nuclear Lamin-A Scales with Tissue Stiffness and Enhances Matrix-Directed Differentiation. Science, 341(6149):1240104, August 2013. [PubMed: 23990565]

[53]. Sandra R Schulze Beatrice Curio-Penny, Li Yuhong, Reza A Imani Lena Rydberg, Pamela K Geyer, and Lori L Wallrath. Molecular Genetic Analysis of the Nested *Drosophila melanogaster* Lamin C Gene. Genetics, 171(1):185–196, September 2005. [PubMed: 15965247]

[54]. Riemer D, Stuurman N, Berrios M, Hunter C, Fisher PA, and Weber K. Expression of Drosophila lamin C is developmentally regulated: analogies with vertebrate A-type lamins. Journal of Cell Science, 108(10):3189–3198, October 1995. [PubMed: 7593280]

[55]. Agrawal Vipin, Pandey Vikash, and Mitra Dhrubaditya. Active buckling of pressurized spherical shells: Monte carlo simulation. arXiv, 2206:14172, 2022.

[56]. Chakrabarti Brato, Liu Yanan, John LaGrone Ricardo Cortez, Fauci Lisa, Olivia du Roure David Saintillan, and Lindner Anke. Flexible filaments buckle into helicoidal shapes in strong compressional flows. Nature Physics, 16(6):689–694, June 2020.

[57]. Loubet Bastien, Seifert Udo, and Michael Andersen Lomholt. Effective tension and fluctuations in active membranes. Physical Review E, 85(3):031913, March 2012.

[58]. Vutukuri Hanumantha Rao, Hoore Masoud, Abaurrea-Velasco Clara, Buren Lennard van, Dutto Alessandro, Auth Thorsten, Fedosov Dmitry A., Gompper Gerhard, and Vermant Jan. Active particles induce large shape deformations in giant lipid vesicles. Nature, 586(7827):52–56, October 2020. [PubMed: 32999485]

[59]. Bausch AR and Kroy K. A bottom-up approach to cell mechanics. Nature Physics, 2(4):231–238, April 2006.

[60]. Hampoelz Bernhard, Yannick Azou-Gros Roxane Fabre, Markova Olga, Puech Pierre-Henri, and Lecuit Thomas. Microtubule-induced nuclear envelope fluctuations control chromatin dynamics in *Drosophila* embryos. Development, 138(16):3377–3386, August 2011. [PubMed: 21752932]

[61]. Deviri Dan and Safran Samuel A.. Balance of osmotic pressures determines the nuclear-to-cytoplasmic volume ratio of the cell. Proceedings of the National Academy of Sciences, 119(21):e2118301119, May 2022.

[62]. Lemière Jöel, Real-Calderon Paula, Holt Liam J, Fai Thomas G, and Chang Fred. Control of nuclear size by osmotic forces in Schizosaccharomyces pombe. eLife, 11:e76075, July 2022. [PubMed: 35856499]

[63]. Cosgrove Brian D., Loebel Claudia, Driscoll Tristan P., Tsinman Tonia K., Dai Eric N., Heo Su-Jin, Dyment Nathaniel A., Burdick Jason A., and Mauck Robert L.. Nuclear envelope wrinkling predicts mesenchymal progenitor cell mechano-response in 2D and 3D microenvironments. Biomaterials, 270:120662, March 2021. [PubMed: 33540172]

[64]. Elosegui-Artola Alberto, Andreu Ion, Beedle Amy E.M., Lezamiz Ainhoa, Uroz Marina, Kosmalska Anita J., Oria Roger, Kechagia Jenny Z., Rico-Lastres Palma, Roux Anabel-Lise Le,

Shanahan Catherine M., Trepat Xavier, Navajas Daniel, Garcia-Manyes Sergi, and Roca-Cusachs Pere. Force Triggers YAP Nuclear Entry by Regulating Transport across Nuclear Pores. Cell, 171(6):1397–1410.e14, November 2017. [PubMed: 29107331]

[65]. Makhija Ekta, Jokhun DS, and Shivashankar GV. Nuclear deformability and telomere dynamics are regulated by cell geometric constraints. Proceedings of the National Academy of Sciences, 113(1):E32–E40, 2016.

[66]. Kelpsch Daniel J., Groen Christopher M., Fagan Tiffany N., Sudhir Sweta, and Tootle Tina L.. Fascin regulates nuclear actin during *Drosophila* oogenesis. Molecular Biology of the Cell, 27(19):2965–2979, October 2016. [PubMed: 27535426]

[67]. Dialynas George, Speese Sean, Budnik Vivian, Geyer Pamela K., and Wallrath Lori L.. The role of *Drosophila* Lamin C in muscle function and gene expression. Development, 137(18):3067–3077, September 2010. [PubMed: 20702563]

[68]. Prasad Mohit and Montell Denise J.. Cellular and Molecular Mechanisms of Border Cell Migration Analyzed Using Time-Lapse Live-Cell Imaging. Developmental Cell, 12(6):997–1005, June 2007. [PubMed: 17543870]

[69]. Schindelin Johannes, Ignacio Arganda-Carreras Erwin Frise, Kaynig Verena, Longair Mark, Pietzsch Tobias, Preibisch Stephan, Rueden Curtis, Saalfeld Stephan, Schmid Benjamin, Tinevez Jean-Yves, Daniel James White Volker Hartenstein, Eliceiri Kevin, Tomancak Pavel, and Cardona Albert. Fiji: an open-source platform for biological-image analysis. Nature Methods, 9(7):676–682, July 2012. [PubMed: 22743772]

[70]. Legland David, Arganda-Carreras Ignacio, and Andrey Philippe. MorphoLibJ: integrated library and plugins for mathematical morphology with ImageJ. Bioinformatics, 32(22):3532–3534, July 2016. [PubMed: 27412086]

[71]. Mietke Alexander. Dynamics of active surfaces. PhD thesis, Technische Universität Dresden, 2018.

[72]. Burns Keaton J., Vasil Geoffrey M., Oishi Jeffrey S., Lecoanet Daniel, and Brown Benjamin P.. Dedalus: A flexible framework for numerical simulations with spectral methods. Physical Review Research, 2(2):023068, April 2020.

[73]. Lin Lawrence C.-L. and Brown Frank L. H.. Brownian Dynamics in Fourier Space: Membrane Simulations over Long Length and Time Scales. Physical Review Letters, 93(25):256001, December 2004. [PubMed: 15697914]

[74]. Reuther Albert, Kepner Jeremy, Byun Chansup, Samsi Siddharth, Arcand William, Bestor David, Bergeron Bill, Gadepally Vijay, Houle Michael, Hubbell Matthew, Jones Michael, Klein Anna, Milechin Lauren, Mullen Julia, Prout Andrew, Rosa Antonio, Yee Charles, and Michaleas Peter. Interactive supercomputing on 40,000 cores for machine learning and data analysis. In 2018 IEEE High Performance extreme Computing Conference (HPEC), pages 1–6. IEEE, 2018.

[75]. Wieczorek Mark A. and Meschede Matthias. SHTools: Tools for Working with Spherical Harmonics. Geochemistry, Geophysics, Geosystems, 19(8):2574–2592, August 2018.

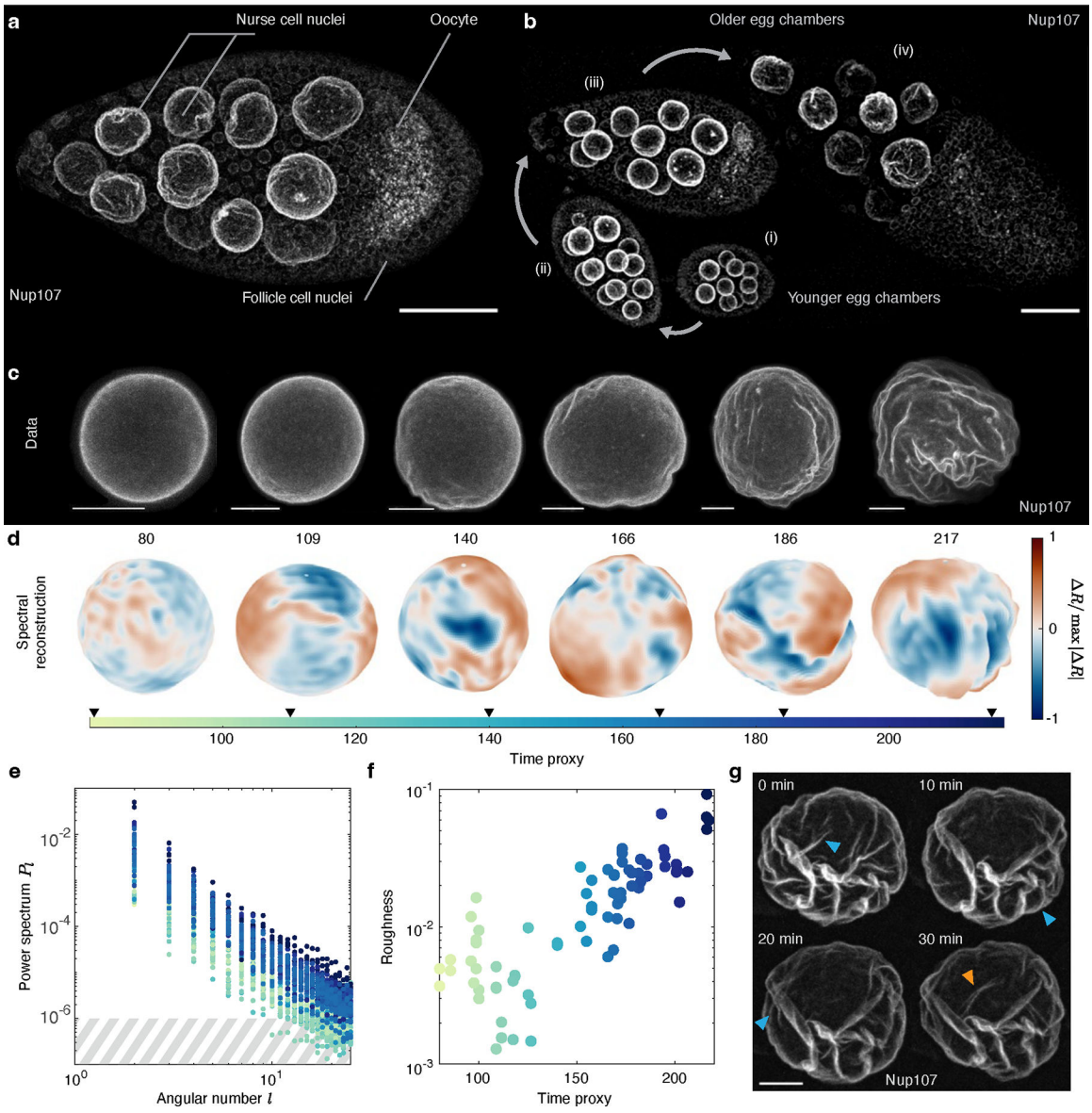

FIG. 1. Dynamic wrinkling of nurse cell nuclear envelopes during *Drosophila* egg development.

a, Maximum-intensity projection (MIP) of a 3D image of an egg chamber expressing GFP-labeled Nup107, a component of the nuclear pore complex. The wrinkled nuclei of the 15 nurse cells are substantially larger than those of the surrounding follicle cells. **b**, MIP of four egg chambers showing an increase in nurse cell nuclear size and nuclear surface deformation as egg chambers age. Curved arrows indicate developmental progression from youngest (i) to oldest (iv). **c**, MIPs of individual nurse cell nuclei from six egg chambers spanning all ages included in our dataset, showing an increase in nuclear radius and NE wrinkling with age. Note that scale bar is the same size for each image; oldest nucleus shown is about 2.3 times the diameter of youngest shown. **d**, Spectral reconstruction of NE surfaces shown in **c** from 3D microscopy data using spherical harmonics with an angular number up to $l_{max} = 25$ (Eq. (1), Methods). Time proxy values for each nucleus are included above

the reconstructions. **e**, Power spectra normalized by average radius for $N = 78$ nuclei from 39 egg chambers in nurse cells directly connected to the oocyte (results are qualitatively similar for nuclei farther away from the oocyte; Supp. Fig. S4). Hashed area indicates approximate noise threshold for young nuclei; color indicates the time proxy (corresponding to the color bar in) as defined in the text and detailed in SI Sec. III 1. **f,** NE roughness $\mathscr{R} = \sum_{l \geq 3}(2l + 1)P_l$ for the same nuclei as in e increases exponentially with time proxy (see also Supp. Fig. S4). g, Snapshots of the same nucleus at four different time points illustrate that NE wrinkling is a dynamic process (Supplementary Video 2). Blue and orange arrowheads point to wrinkles that disappear and appear, respectively, between subsequent frames. Scale bars: 50 μm (**a**, **b**), 10 μm (**c**, **g**).

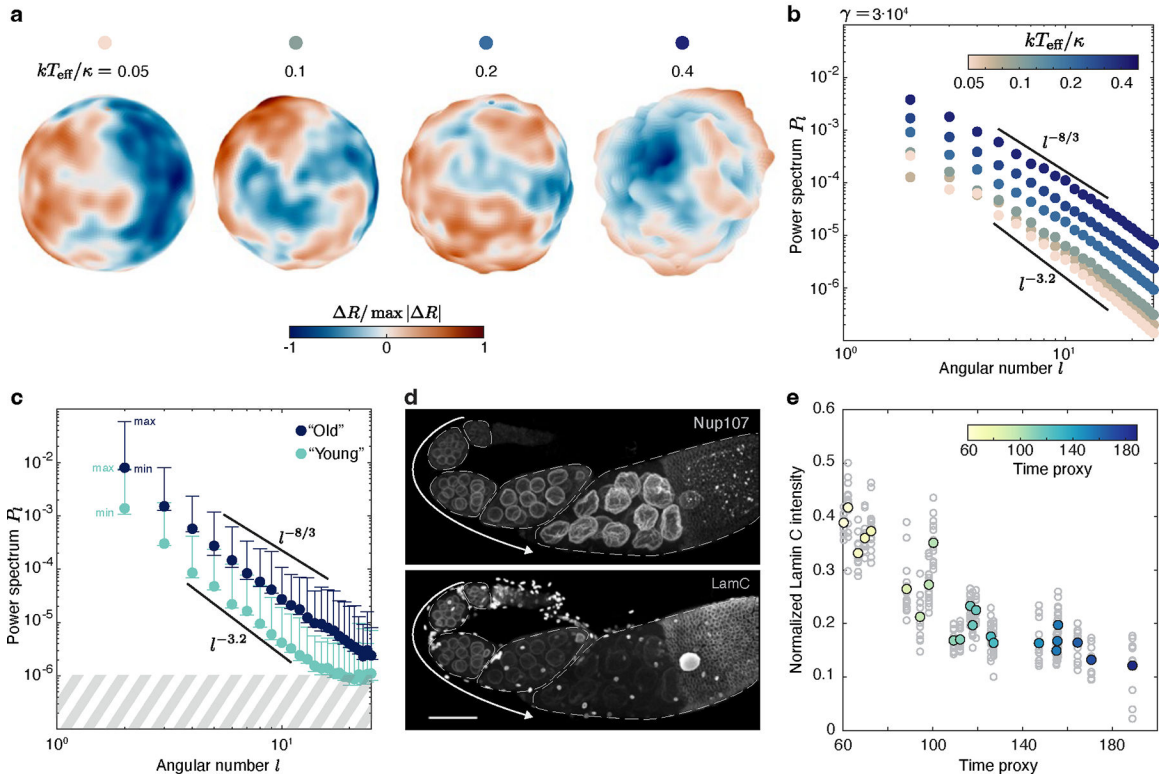

FIG. 2. Fluctuating elastic shell theory predicts a scaling law with exponent ≈ 3 for the wrinkle power spectrum, in agreement with experiments.

a, Equilibrium simulation snapshots of nuclei at temperature $T_{\text{eff}} = 10T_{\text{eq}}$, undeformed radius $R = 25\ \mu$m and $R_c/R = 20$, at fixed FvK number $\gamma = 3 \times 10^4$ for varying elastic moduli controlled by kT_{eff}/κ. Color indicates the normalized deviation of the surface from the mean shell radius. **b**, Time-averaged spectra of simulated NEs of undeformed radius $R = 25\ \mu$m, $R_c/R = 20$, $T_{\text{eff}} = 10T_{\text{eq}}$ for different moduli κ, Y at fixed $\gamma = 3 \times 10^4$, showing the transition from weak nonlinearity to strong nonlinearity as bending rigidity decreases. Color bar matches the dots from **a. c**, Binned averages of spectra from nuclei in nurse cells directly connected to the oocyte reveal that shape fluctuations follow a scaling law with an exponent between −3.2 and −8/3 that is obeyed throughout development. 'Young' nuclei have a time proxy between 80–140, $N = 29$ nuclei, 12 egg chambers; 'Old' nuclei have a time proxy between 160–220, $N = 40$ nuclei, 22 egg chambers. Bars show extremal values. Hashed area indicates approximate noise threshold for young nuclei. (See Supp. Fig. S4 for comparison between nuclei at different positions in the egg chamber) **d**, Fixed egg chambers expressing Nup107::RFP and stained for Lamin C, showing a decrease in Lamin C intensity in nurse cell nuclei as egg chambers increase in age. In contrast, Nup107::RFP intensity stays relatively constant. The same trend is observed in live imaging of egg chambers expressing LamC::GFP and Nup107::RFP (Supp. Fig. S6a). Wrinkling of nuclei in younger egg chambers (all but the rightmost) results from fixation and is not observed in live imaging until later stages. Arrows indicate increasing age; egg chamber boundaries are shown in

dashed outlines. Scale bar: 50 μm. e, Normalized Lamin C fluorescence intensity decreases approximately 5-fold over time. Normalization details are specified in the Methods. $N = 337$ nuclei from 23 egg chambers; colored dots show means for each egg chamber.

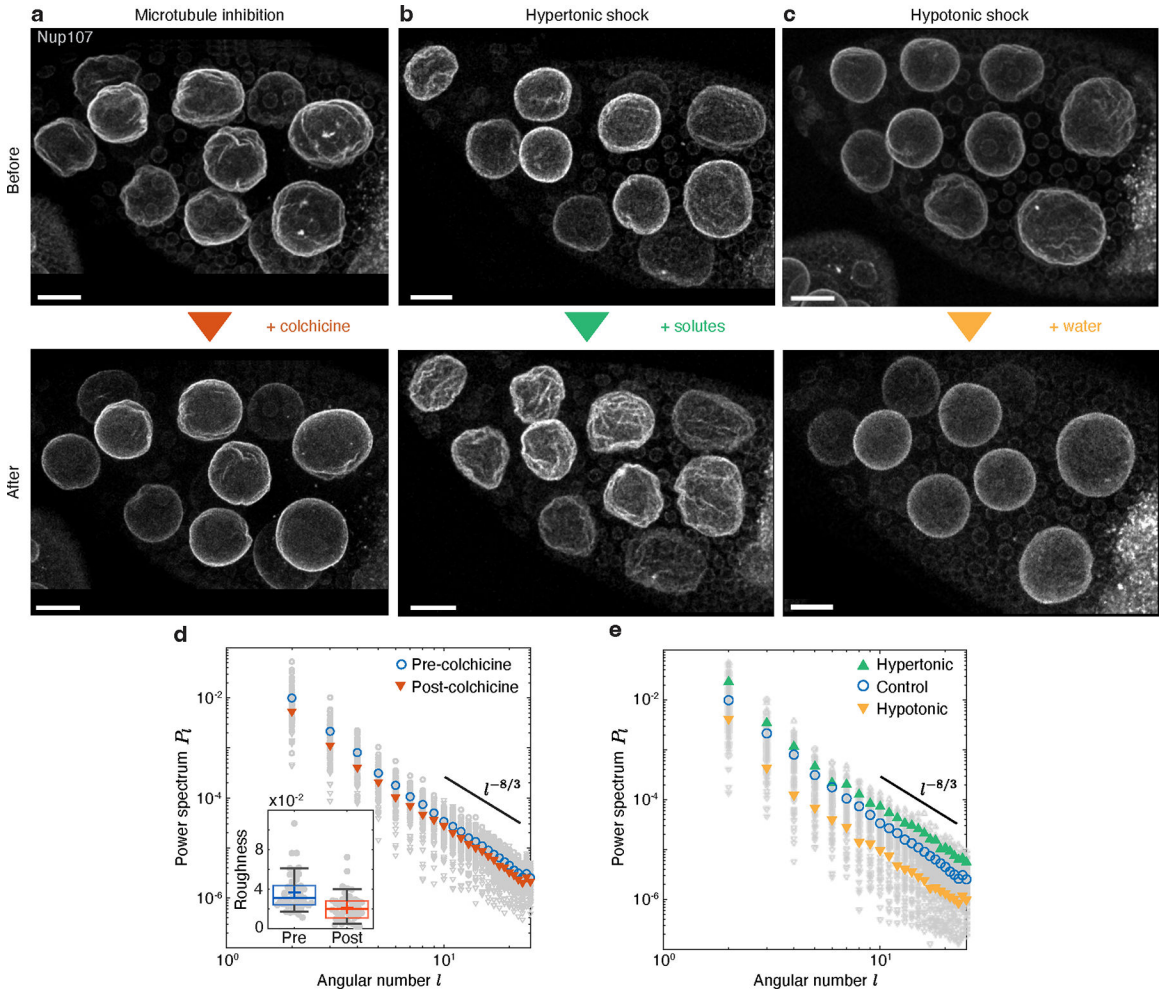

FIG. 3. Perturbation experiments confirm robustness of observed scaling laws and reveal NE wrinkling reversal mechanisms.

a, MIP of one egg chamber before (top) and after (bottom) inhibition of microtubule polymerization by colchicine, showing that microtubule disruption can reverse wrinkling (Supplementary Video 4). **b**, MIPs before and after hypertonic shock using an external culture medium of 1.5x osmolarity, showing an increase in wrinkling. c, MIPs before and after hypotonic shock using an external culture medium of 0.5x osmolarity, showing a decrease in wrinkling. Egg chambers in **a**, **b**, and **c** have time proxies of 171, 174, and 171, respectively. **d**, The power spectrum after microtubule inhibition by colchicine still follows a power law with roughly the same exponent, with a reduction of roughness by a factor of 2 (inset). $N = 49$ pre-colchicine and post-colchicine nuclei, from 6 egg chambers, time proxies 169–182. For box plots, plus signs denote mean, middle line is the median, top and bottom edges of the box are the upper and lower quartiles, and whiskers span from 9% to 91% of the data range. **e**, In the presence of increased inwards (hypertonic) or outwards (hypotonic) pressure, the overall shape of the power spectrum remains approximately conserved. Hypotonic shock treatment reduces the wrinkle amplitudes, providing a reversal mechanism for NE wrinkling. Spectra were computed using 49 control, 15 hypertonic, and 30 hypotonic nuclei in the time proxy range 165–185, from 6,3, and 6 egg chambers,

respectively, using nuclei from all nurse cells rather than only those directly connected to the oocyte. Supp. Fig. S7 shows roughness values over a larger range of time proxies. Scale bars: 20 μm.